Chinese Chemical Letters 33 (2022) 1459–1462

Contents lists available at ScienceDirect

Chinese Chemical Letters

journal homepage: www.elsevier.com/locate/cclet

Molecular self-induced configuration for improving dissymmetry factors in tetradentate platinum(II) enantiomers cycloaddition

Li Yuan[a], Qian-Jun Ding[a], Zhen-Long Tu[a], Xiang-Ji Liao[a], Xu-Feng Luo[a], Zhi-Ping Yan[a], Zheng-Guang Wu[b,*], You-Xuan Zheng[a,*]

[a] State Key Laboratory of Coordination Chemistry, School of Chemistry and Chemical Engineering, Nanjing University, Nanjing 210023, China
[b] Nantong Key Lab of Intelligent and New Energy Materials, College of Chemistry and Chemical Engineering, Nantong University, Nantong 226019, China

ARTICLE INFO

Article history:
Received 28 July 2021
Revised 18 August 2021
Accepted 23 August 2021
Available online 28 August 2021

Keywords:
Pt(II) enantiomer
Circularly polarized luminescence
Dissymmetry factor
Molecular self-induction
Helicene-like structure

ABSTRACT

Two pairs of Pt(II) enantiomers ((*RR*)/(*SS*)-PyPt, ((*RR*)/(*SS*)-Py: *N,N'*-(1,2-diphenylethane-1,2-diyl)dipicolinamide; (*RR*)-*P*/*M*-QPt, ((*RR*)/(*SS*)-Q: *N,N'*-((1*R*,2*R*)-1,2-diphenylethane-1,2-diyl)bis(quinoline-2-carboxamide)) were synthesized, respectively, with good circularly polarized luminescence (CPL) and tunable dissymmetry factors (*g*) by molecular self-induction with (*RR*)/(*SS*)-1,2-diphenylethane-1,2-diamine as carbon chiral sources. In the (*RR*)-*P*-QPt and (*SS*)-*M*-QPt, specific *P*- and *M*-configurations were effectively induced from intrinsic chiral carbon centres (*R* or *S*), ingeniously avoiding the racemic mixture formation and chiral separation. Furthermore, the chirality originating from both chiral carbon centres and helicene-like structure improves the *g* factor significantly, which provides a new molecular design strategy for chiral Pt(II) enantiomers with good CPL properties.

Circularly polarized light (CPL) possesses potential application in CP organic light-emitting diode (CP-OLED) and 3D display, optical data storage and optical spintronic [1,2]. Circular dichroism (CD) and CPL spectra are two main detection methods for chiral materials. The CD spectrum can be employed to analyse the configuration of chiral molecules at their ground states, while CPL is used for studying chiral characteristics of their excited states. The optical activity intensity of chiral materials can be characterized by dissymmetry factor (g), and the absorption g_{abs} factor is defined as $g_{abs} = \Delta\varepsilon/\varepsilon = 2(\varepsilon_L - \varepsilon_R)/(\varepsilon_L + \varepsilon_R)$, where ε_L and ε_R indicate molar absorption coefficients of left and right absorption, respectively. The luminescent g_{lum} factor is defined as $g_{lum} = 2\Delta I/I = 2(I_L - I_R)/(I_L + I_R)$, while I_L and I_R represent the left and right CPL intensities. There is no circular polarization with the g factor of zero, whereas factors of $+2$ and -2 refer to ideal highest left- or right-handed CPL, respectively. Originally, CPL can be obtained by a complicated device architecture with 1/4 slide and polarizer, resulting in brightness loss. Therefore, it is imperative to develop chiral emitters that can generate CPL directly.

In most cases, there are two main molecular design strategies for chiral luminophores: introducing stereoselectivity to realize the separation of enantiomers or endowing the molecule structure with chiral units. Carbon [3-7], axial [8-16], planar [17-20] and helical [21-23] chiral sources were commonly used. But generally, chiral carbons in these molecules are far away from luminescence centre, which do not affect CPL properties greatly. Therefore, the g factors of these materials are at relatively low grade. Aside from chiral carbon, binaphthol derivatives with axial chirality is also often employed as well [8-15]. However, these materials have same drawbacks as carbon chiral materials. Notably, helicenes do not have any asymmetric carbon centres, whereas their twisted and extended π-conjugated molecular structures exhibit the special helical chirality and excellent CPL properties.

However, the synthesis of helicene usually suffered from harsh reaction conditions and cumbersome operation. Moreover, the helicene-based enantiomers can be basically obtained from racemates through chiral resolution, making the preparation and separation process complicated. Therefore, developing a concise and efficient method to directly construct helical molecules with high dissymmetry factor without resolution remains a significant challenge.

Among all these chiral materials, traditional fluorescent materials can use only 25% of singlet excitons formed during the exciton recombination process, which results in lower CP-OLED efficiency. Notably, phosphorescent complexes can utilize both singlet and triplet excitons to improve the internal quantum efficiency (IQE) up to 100%. Although these materials show better device efficiency, the reported g factors based on transition metal (Ir(III)

* Corresponding authors.
E-mail addresses: wuzhengguang_zy@163.com (Z.-G. Wu), yxzheng@nju.edu.cn (Y.-X. Zheng).

https://doi.org/10.1016/j.cclet.2021.08.104
1001-8417/

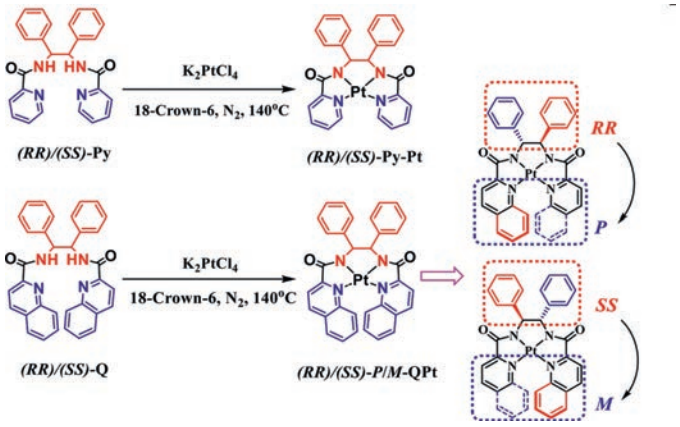

Fig. 1. Design strategy and synthetic routes of chiral tetradentate Pt(II) complexes.

[24-26] or Pt(II) [27-33]) complexes are at 10^{-3} -10^{-2} order, which still leaves much to be desired.

Herein, two pairs of chiral tetradentate Pt(II) complex (Fig. 1) were synthesized using chirality induction strategy to obtain high *g* factors. The chirality of (*RR*)/(*SS*)-PyPt ((*RR*)/(*SS*)-Py: *N,N'*-(1,2-diphenylethane-1,2-diyl)dipicolinamide) is only inherited from chiral (*RR*)/(*SS*)-1,2-diphenylethane-1,2-diamine. But the chirality of (*RR*)-*P*-QPt and (*SS*)-*M*-QPt ((*RR*)/(*SS*)-Q: *N,N'*-((*1R,2R*)-1,2-diphenylethane-1,2-diyl)bis(quinoline-2-carboxamide)) originates from chiral carbon centres as well as a helicene-like structure during the platinum coordination process. It is worth noting that the $|g_{PL}|$ factors of (*RR*)-*P*-QPt and (*SS*)-*M*-QPt are significantly improved to around 3.5×10^{-3}, five times higher than that of (*RR*)/(*SS*)-PyPt. In the (*RR*)-*P*-QPt and (*SS*)-*M*-QPt structures, the specific *P*- and *M*-configurations result from intrinsic chiral carbon centre, ingeniously avoiding the formation of racemic mixture, which means future chiral separation is of no need.

The synthetic routes of the target chiral tetradentate Pt(II) complexes and the synthesis details are provided in Supporting information. Commercially available chiral 1,2-diphenylethane-1,2-diamine is employed as reactant and the final products were obtained through only two steps. For (*RR*)-*P*-QPt and (*SS*)-*M*-QPt enantiomers, the reactant with *S*-configuration can only form *M*-configuration specifically, avoiding enantio-separation. Therefore, the newly chirality is born from steric hindrance effect after Pt(II) ion coordination with ligand. As revealed by the thermogravimetric analysis curves (Figs. S10 and S11 in Supporting information), the decomposition temperatures are 333 and 347 °C, respectively, demonstrating the high thermal stability of these Pt(II) complexes.

As shown in Fig. 2, the single crystal diffraction analysis well confirmed the preconceived molecular structures. In the structures of (*RR*)/(*SS*)-PyPt, Pt(II) adopts the form of plane tetragonal coordination without any other steric hinderance existing, therefore, the planes of pyridine and the three coordinated five-membered rings are almost parallel. In (*RR*)-*P*-QPt and (*SS*)-*M*-QPt, Pt(II) ion adopts analogous coordinative form, but with the steric hinderance caused by two quinoline units on each side, thus the enantiomers present more twisted structures with the angle between the two planes of quinoline is 38.3°, which is similar to the reported value in [7]helicene (hc ≈ 30.7°) [34].

Furthermore, (*RR*)-*P*-QPt and (*SS*)-*M*-QPt enantiomers form new spiral structures after coordination, which would effectively enhance their CPL properties and *g* factors. Besides, as shown in Fig. S9 (Supporting information), the phenyl group attached to the chiral carbon and the quinoline unit at the same side must be spatially away from each other due to the steric hindrance in order to have a more stable configuration. If there were no phenyl groups existing, it should form four isomers, namely (*SS*)-*P*-QPt, (*SS*)-*M*-QPt, (*RR*)-*P*-QPt and (*RR*)-*M*-QPt. Therefore, the specific configurations of (*RR*)-*P*-QPt and (*SS*)-*M*-QPt enantiomers are induced by this special structure, avoiding further enantio-separation.

In CH_2Cl_2 solutions (5×10^{-5} mol/L) at room temperature, these Pt(II) complexes show strong absorption bands in the region of 250–350 nm (Fig. 3), which are attributed to the spin-allowed singlet $\pi-\pi^*$ transitions of ligands. Due to the strong spin-orbital coupling effect of the Pt(II), the absorption spectra of the complexes also show a wide band ranging from 350 nm to 500 nm, which belong to the mixed singlet and triplet MLCT (metal-to-ligand charge-transfer) transitions. Alternatively, the location of the transition can also be simulated by theoretical calculations (Table S9 in Supporting information). For example, the excited state from S_0 to S_1 transition of (*RR*)-*P*-QPt is dominated by HOMO-LUMO transition, which is generated by the large conjugate quinoline system with the Pt(II) centre (Fig. S32 in Supporting information).

In addition, the photoluminescence spectra of (*RR*)/(*SS*)-PyPt at room temperature demonstrate the main emission peak at 564 nm with the Commission Internationale de L'Eclairage (CIE) coordinates of (0.44, 0.54). While the photoluminescence spectra of (*RR*)-*P*-QPt and (*SS*)-*M*-QPt display the main emission peak at 616 nm with the CIE coordinates of (0.63, 0.37). Therefore, the replacement of pyridine by quinoline would result in emission red-shift of the Pt(II) enantiomers. When measured at 77 K, the emission peak of (*SS*)-PyPt is shifted to 503 nm with a shoulder peak at 534 nm. Similarly, the emission peak of (*SS*)-*M*-QPt is moved to 594 nm with a shoulder peak at 634 nm, which could be assigned to ^{1}MLCT and ^{3}MLCT transitions [15], respectively. The absolute photoluminescence quantum yields (PLQYs) of (*RR*)/(*SS*)-PyPt and (*RR*)/(*SS*)-*P/M*-QPt are 6.72% and 1.99% with lifetimes of 0.14 and 0.11 μs in CH_2Cl_2 solutions, PLQYs of 0.13 and 0.04 with lifetimes of 0.19 and 0.18 μs in neat films, respectively. The PLQYs are not as high as we expected.

To further characterize the chiroptical properties of two pairs of (*RR*)/(*SS*)-PyPt and (*RR*)/(*SS*)-*P/M*-QPt enantiomers, the CD and CPL spectra were investigated. As illustrated in Figs. 4a and d, clear mirror-image CD spectra of the two pairs of enantiomers are observed with alternating positive and negative Cotton effects. (*RR*)-PyPt shows a clear positive Cotton effects at 262 and 350 nm, and negative Cotton effects at 300 and 390 nm, whereas (*SS*)-PyPt displays the opposite signals at the same positions. The (*RR*)-*P*-QPt and (*SS*)-*M*-QPt demonstrate similar mirror symmetric CD spectra as (*RR*)/(*SS*)-PyPt with commutative positive and negative Cotton effects. The intense Cotton effects in short-wavelength regions are assigned to absorption caused by the intramolecular π-system CT, while the Cotton effects at the long-wavelength absorption bands are caused by the MLCT processes.

As for the CPL spectra and g_{PL} versus wavelength curves (Figs. 4b, c, e and f), (*RR*)-PyPt and (*SS*)-PyPt show symmetrical spectra at 470-700 nm with the g_{PL} factors of $-0.77/+0.63 \times 10^{-3}$ in CH_2Cl_2 solutions. Similarly, (*RR*)-*P*-QPt and (*SS*)-*M*-QPt also display symmetrical spectra at 480-750 nm. Notably, g_{PL} factors of (*RR*)-*P*-QPt and (*SS*)-*M*-QPt are significantly improved to -3.5×10^{-3} and $+3.1 \times 10^{-3}$, almost five times higher than that of (*RR*)-PyPt and (*SS*)-PyPt, owing to the formation of the spiral chiral centres in (*RR*)-*P*-QPt and (*SS*)-*M*-QPt enantiomers. This phenomenon can be confirmed by the crystal packing structures of the enantiomers (Fig. 2c).

Furthermore, the definition of *g* factor is given in

$$g = \Delta I/(I/2) = 2(I_L - I_R)/(I_L + I_R) = 4\,\vec{\mu}\cdot\vec{m}\,/\left(|\,\vec{\mu}\,|^2 + |\,\vec{m}\,|^2\right) \quad (1)$$

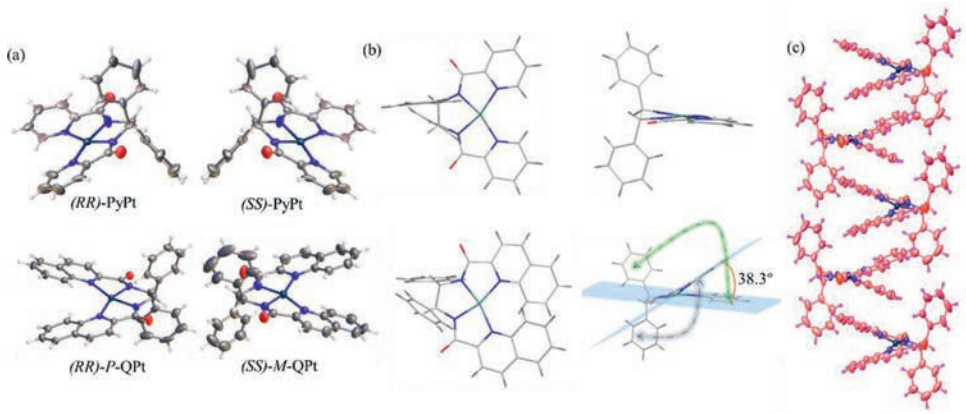

Fig. 2. (a) Crystal structures of the enantiomers of (*RR*)-PyPt (CCDC:2078749), (*SS*)-PyPt (CCDC:2083860), (*RR*)-*P*-QPt (CCDC: 2073874) and (*SS*)-*M*-QPt (CCDC: 2073866). (b) The topview and sideview of (*RR*)-PyPt and (*RR*)-*P*-QPt. (c) Crystal packing of (*RR*)-*P*-QPt.

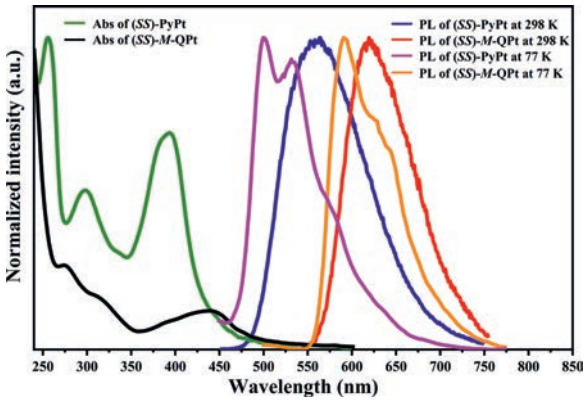

Fig. 3. Normalized absorption and emission spectra of (*SS*)-PyPt, (*SS*)-*M*-QPt in CH_2Cl_2 solutions.

where $\vec{\mu}$ and $\vec{m}$ indicate the electric and magnetic dipole transition moments, respectively. According to the equation, the equal $|\vec{m}|$ and $|\vec{\mu}|$ factors of the material would cause the biggest *g* factor colse to 2. But in most chiral materials, except for lanthanide complexes, the $|\vec{m}|$ data are much lower than that of $|\vec{\mu}|$. Therefore, most chiral materials only show low *g* factors, less than 10^{-2} order in most cases.

For these complexes, the theoretically calculated electric dipole moment $\vec{\mu}$ factors of (*RR*)-PyPt from S_0 to S_1 transition is (0.0009, −0.1459, 0.0003), and the magnetic dipole moment $\vec{m}$ is (0, −0.0093, −0.0001), thus the $|\vec{\mu}|$ and $|\vec{m}|$ data are 0.1459 and 0.0093 respectively (Figs. S28–S31 and Tables S4–S8 in Supporting information). However, for the (*RR*)-*P*-QPt, the theoretically calculated electric dipole moment $\vec{\mu}$ from S_0 to S_1 transition is (−0.0289, −0.0082, −0.0092), and the magnetic dipole moment $\vec{m}$ is (0.0812, −0.0009, −0.0328), thus the $|\vec{\mu}|$ and $|\vec{m}|$ factors are 0.0314 and 0.088, respectively. It is obvious that (*RR*)-*P*-QPt has a smaller $|\vec{\mu}|$ and a bigger $|\vec{m}|$ than that of (*RR*)-PyPt, which can explain why it has higher *g* factor than that of (*RR*)-PyPt. Besides, the calculated g_{abs} factor of (*RR*)-PyPt from S_0 to S_1 transition is positive, in accordance with the positive signal of CD spectrum at long-wavelength region. And the calculated g_{abs} factor of (*RR*)-*P*-QPt from S_0 to S_1 transition is negative, also in accordance with the negative signal of CD spectrum at long-wavelength region (Table S8).

In conclusion, two pairs of chiral tetradentate Pt(II) enantiomers were synthesized simply by a two-step reaction employing com-

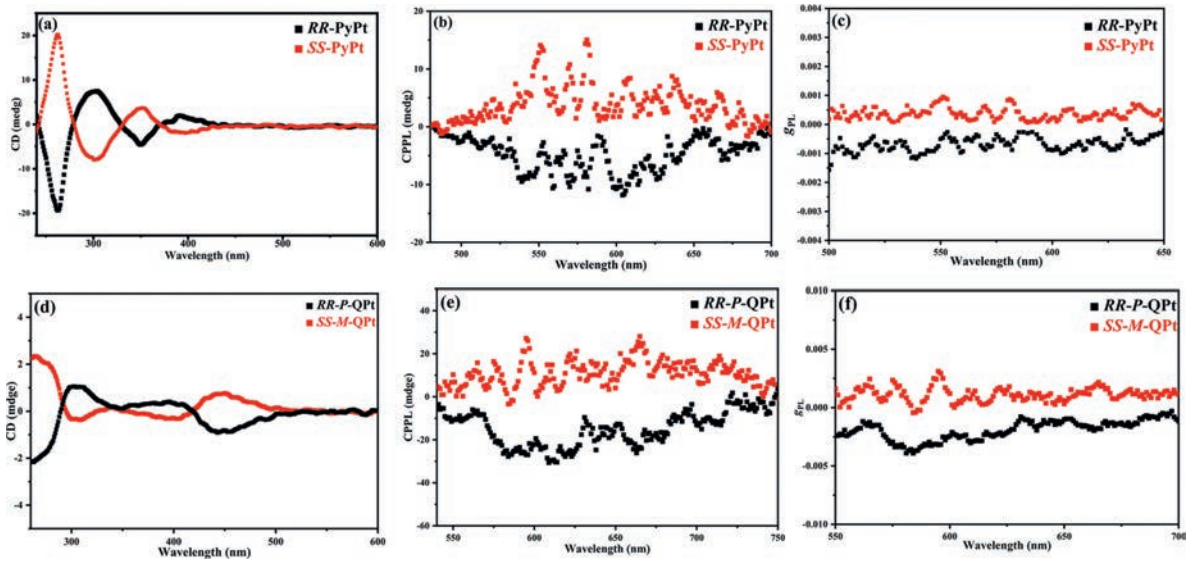

Fig. 4. (a) CD spectra of (*RR*)/(*SS*)-PyPt, (b) CPL spectra of (*RR*)/(*SS*)-PyPt, (c) g_{PL} versus wavelength curves of (*RR*)/(*SS*)-PyPt, (d) CD spectra of (*RR*)-*P*-QPt and (*SS*)-*M*-QPt, (e) CPL spectra of (*RR*)-*P*-QPt and (*SS*)-*M*-QPt, (f) g_{PL} versus wavelength curves of (*RR*)-*P*-QPt and (*SS*)-*M*-QPt in CH_2Cl_2 solutions.

mercially available reactant. In (*RR*)-*P*-QPt and (*SS*)-*M*-QPt, the new spiral chiral centre with specific configuration was induced by the platinum coordination, which not only avoid the chiral separation process, but also greatly improve the *g* factors from $-0.77/+0.63 \times 10^{-3}$ to $-3.5/+3.1 \times 10^{-3}$ due to the original chiral carbon centres and formed helical-like structure. This improved *g* factors phenomenon was confirmed by the enantiomers' single crystal structures and the theoretical electric and magnetic dipole transition moments calculation. This work provides a new molecular design strategy for Pt(II) enantiomers with good CPL properties and high *g* factors.

Declaration of competing interest

The authors declare that they have no known competing financial interests or personal relationships that could have appeared to influence the work reported in this paper.

Acknowledgment

This research is supported by the National Natural Science Foundation of China (Nos. 51773088 and 21975119).

Supplementary materials

Supplementary material associated with this article can be found, in the online version, at doi:10.1016/j.cclet.2021.08.104.

References

[1] D.W. Zhang, M. Li, C.F. Chen, Chem. Soc. Rev. 49 (2020) 1331–1343.
[2] L. Frédéric, A. Desmarchelier, L. Favereau, G. Pieters, Adv. Funct. Mater. 31 (2021) 2010281.
[3] T. Imagawa, S. Hirata, K. Totani, et al., Chem. Commun. 51 (2015) 13268–13271.
[4] M. Li, S.H. Li, D. Zhang, et al., Angew. Chem. Int. Ed. 57 (2018) 2889–2893.
[5] F.Y. Hao, Y.Z. Shi, K. Wang, et al., Dyes Pigm. 178 (2020) 108336.
[6] S.Y. Yang, Y.K. Wang, C.C. Peng, et al., J. Am. Chem. Soc. 142 (2020) 17756–17765.
[7] F. Ni, C.W. Huang, Y. Tang, et al., Mater. Horiz. 8 (2021) 547–555.
[8] S. Feuillastre, M. Pauton, L. Gao, et al., J. Am. Chem. Soc. 138 (2016) 3990–3993.
[9] F. Song, Z. Xu, Q. Zhang, et al., Adv. Funct. Mater. 28 (2018) 1800051.
[10] S. Sun, J. Wang, L. Chen, et al., J. Mater. Chem. C 7 (2019) 14511–14516.
[11] Z.G. Wu, H.B. Han, Z.P. Yan, et al., Adv. Mater. 31 (2019) 1900524.
[12] Y. Wang, Y. Zhang, W. Hu, et al., ACS Appl. Mater. Interfaces 11 (2019) 26165–26173.
[13] L. Frédéric, A. Desmarchelier, R. Plais, et al., Adv. Funct. Mater. 30 (2020) 2004838.
[14] Y. Xu, Q. Wang, X. Cai, et al., Adv. Mater. 33 (2021) 2100652.
[15] F.M. Xie, J.X. Zhou, X.Y. Zeng, et al., Adv. Opt. Mater. 9 (2021) 2100017.
[16] M. Li, Y.F. Wang, D. Zhang, et al., Angew. Chem. Int. Ed. 59 (2020) 3500–3504.
[17] M.Y. Zhang, Z.Y. Li, B. Lu, et al., Org. Lett. 20 (2018) 6868–6871.
[18] N. Sharma, E. Spuling, C.M. Mattern, et al., Chem. Sci. 10 (2019) 6689–6696.
[19] C. Liao, Y. Zhang, S.H. Ye, W.H. Zheng, ACS Appl. Mater. Interfaces 13 (2021) 25186–25192.
[20] Y. Xu, Q. Wang, X. Cai, et al., Adv. Mater. 33 (2021) 2100652.
[21] H. Sakai, T. Kubota, J. Yuasa, et al., J. Phys. Chem. C 120 (2016) 7860–7869.
[22] T. Otani, A. Tsuyuki, T. Iwachi, et al., Angew. Chem. Int. Ed. 56 (2017) 3906–3910.
[23] Z. Qiu, C.W. Ju, L. Frederic, et al., J. Am. Chem. Soc. 143 (2021) 4661–4667.
[24] T.Y. Li, Y.M. Jing, X. Liu, et al., Sci. Rep. 5 (2015) 14912.
[35] N. Hellou, M.S. Hooper, L. Favereau, et al., Angew. Chem. Int. Ed. 56 (2017) 8236–8239.
[26] J. Han, S. Guo, J. Wang, et al., Adv. Opt. Mater. 5 (2017) 1700359.
[27] J.R. Brandt, X. Wang, Y. Yang, et al., J. Am. Chem. Soc. 138 (2016) 9743–9746.
[28] N. Hellou, M. Srebro-Hooper, L. Favereau, et al., Angew. Chem. Int. Ed. 56 (2017) 8236–8239.
[29] T. Biet, T. Cauchy, Q. Sun, et al., Chem. Commun. 53 (2017) 9210–9213.
[30] G. Fu, Y. He, W. Li, et al., J. Mater. Chem. C 7 (2019) 13743–13747.
[31] Z. Jiang, J. Wang, T. Gao, et al., ACS Appl. Mater. Interfaces 12 (2020) 9520–9527.
[32] G.W. Qian, X.F. Yang, X.B. Wang, et al., Adv. Optical Mater. 8 (2020) 2000775.
[33] J. Hong, S. Kim, G. Park, et al., Chem. Sci. 7 (2021) 8668–8681.
[34] Y. Shen, C.F. Chen, Chem. Rev. 112 (2012) 1463–1535.